Dissociation and sticking of H_2 on the Ni(111), (100), and (110) substrate

Georg Kresse
Institut für Materialphysik, Universität Wien, A-1090 Wien, Austria
(Received 5 April 2000)

The adsorption, dissociation, and sticking of H_2 on the Ni(111), (100), and (110) substrates are studied with spin-polarized gradient corrected density functional theory. To parametrize the six-dimensional (6D) potential energy surface (PES), between six and twelve two-dimensional sections of the PES are calculated using density functional theory. For the interpolation between such 2D sections, a scheme is developed and tested predicting the energy of the H_2 molecules with an accuracy of about 50 meV in low-symmetry sites. On the interpolated 6D PES, classical simulations of the H_2 sticking coefficient are performed, and the results are compared with experiment. The important experimental trends are well reproduced, and a simple model is discussed to explain why dissociation is activated on the (111) surface and nonactivated on the rough (110) surface. The results are compared to those for H_2 on Pd, and it is shown that the difference between Ni and Pd stems mainly from the surface *s* electrons.

I. INTRODUCTION

To understand H_2 adsorption and dissociation on low-index metal surfaces is the first step toward the modeling of more complex catalytic reactions on surfaces. It is therefore not astonishing that the last decade has seen a great effort devoted to the investigation of these processes, leading to a significantly improved understanding of the dissociation reaction. Until recently, most numerical studies were restricted to simple model systems, but with advances in computer performance six-dimensional (6D) quantum-mechanical (QM) simulations of the sticking coefficient on realistic potential energy surfaces (PES's) became feasible. In the first calculations of this character, the 6D PES's of H_2 on Pd(100) and W(100) were derived directly from density functional calculations[1–3] and subsequently used in five- and six-dimensional QM calculations of the sticking coefficient.[4,5] The insight gained from these simulations was significant, because they showed that the experimentally observed decrease of the sticking coefficient with increasing beam energy[6,7] can be explained by steering and not by a precursor mediated process, as often assumed before: at low kinetic energies, molecules are directed by the PES toward favorable adsorption sites, where dissociation readily occurs, whereas at intermediate kinetic energies, the molecules have not sufficient time to reorient or move toward favorable sites, so that they tend to be reflected by the surface.

Despite the insight gained from simulations on realistic PES's, some deficiencies presently remain. One must question in particular whether the functional forms used in the parametrization of the 6D PES are sufficiently flexible to account for all features of the real PES. The current parametrizations often neglect that molecules will be neither exactly parallel to the surface nor upright above low-symmetry sites. In this work, I aim to remove this shortcoming by developing a parametrization that is free of this approximation. Similar to previous approaches,[4,5] the present method is based on accurate first-principles calculations of two-dimensional (2D) sections of the 6D PES at high-symmetry sites. But, in contrast to previous work, the interpolation between such sections is done after subtracting the potential experienced by two isolated H atoms, located at the same positions as the atoms in the H_2 molecule. The resulting functions are smooth and weakly site dependent so that a straightforward interpolation between different adsorption sites becomes physically meaningful.

The approach is applied to the dissociation and sticking of H_2 on low-index Ni surfaces. This choice is mainly motivated by the fact that reliable sticking coefficients were measured experimentally by molecular beam experiments for all three low-index surfaces, allowing for a direct comparison with experiment.[7] Another reason for this choice is the remarkable difference between the three low-index Ni surfaces. On the rough (110) surface, Rendulic *et al.* found a nonactivated behavior, whereas a typical activated normal energy scaling sticking curve was measured for the (111) surface.[7] The exact reason for this behavior is still unclear.

Since the experimentally observed features make Ni a promising candidate for simulations of the sticking coefficient, many studies have been reported before using classical[8–10] and quantum calculations.[11–13] Unfortunately most of these studies suffer from inaccurate potential energy surfaces relying often on the London-Eyring-Polanyi-Sato (LEPS) potentials (see, e.g., Ref. 12 and references therein). As already mentioned, the PES's of the present work are derived from first-principles calculations avoiding any *ad hoc* assumptions. In combination with the interpolation, an accurate and reliable description of the 6D PES is obtained. On the interpolated PES's, the sticking coefficients are evaluated using classical simulations. QM simulations are postponed to later work, since they are very time consuming for the present parametrization. The restriction to classical simulations is certainly the most significant approximation of the current work, but recent calculations show that qualitative trends can be reliably predicted with such simulations.[14,15]

The present work is a comprehensive study of H_2 adsorption, dissociation, and sticking on three different low-index surfaces. Since such systematic investigations are helpful to understand general trends, the differences between the three

surfaces are discussed in detail, and a coherent picture is presented that explains why sticking is nonactivated on the (110) surface and activated on the (111) surface. The results for Ni are compared to those for Pd, where experiments suggest that H_2 dissociation is nonactivated on all three low-index surfaces. The present first-principles calculations suggest, in agreement with experiments, that Ni is generally less reactive than Pd for H_2 dissociation. This is remarkable since simple models relying only on the center of the *d* band predict a different behavior (see, eg., Refs. 16 and 17), and to explain this result one has to consider the metal *s* electrons.

The article is organized as follows. I first discuss the methods used throughout the work, paying particular attention to the parametrization and interpolation of the 6D energy surface. In Sec. III A, the first-principles calculations for 2D sections of the 6D energy surface are presented. The accuracy of the interpolation procedure is tested in Secs. III B and III C, and the final sticking curves are presented in Sec. III D. I finish with a discussion and conclusions.

II. METHOD OF CALCULATION

A. First-principles calculations

The first-principles calculations are based on density functional theory (see, e.g., Refs. 18 and 19) and employ a plane wave basis set.[20,21] To solve the Kohn-Sham equations the Vienna *ab initio* simulation package[22,23] (VASP) is used, which performs an iterative solution of Kohn-Sham equations via an unconstrained band-by-band minimization of the norm of the residual vector of each eigenstate and an optimized charge density mixing. The electron-ion interaction is described by the projector augmented wave (PAW) method as proposed by Blöchl.[24] This method is a frozen core all-electron method, and has the advantage that the exact shape of the valence wave functions is taken into account. This in turn improves the description of magnetic materials considerably.[25] The PAW potentials for Ni and H are similar to those proposed and tested in Refs. 25 and 26. The energy cutoff was set to 270 eV. In all calculations, the generalized gradient approximation of Perdew and co-workers[27,28], commonly refered to as PW91 is used. The slab supercell approach with periodic boundaries is employed to model the surface, and the Brillouin zone sampling is based on the Monkhorst-Pack technique.[29] For the calculation of the fractional occupancies a broadening approach of Methfessel and Paxton[30] with $N=1$ and $\sigma=0.2$ eV is used.

Surface relaxation was not taken into account in any of the present calculations. Tests for atomic H on Ni low-index surfaces, presented in Ref. 26, indicate that this is a very reasonable approximation, errors being about 20 meV.

B. Modeling the Ni surfaces

The (100) and (111) surfaces are modeled by four layers, whereas the (110) surface is described by a five-layer slab. For atomic hydrogen, tests have been presented in previous work[26] demonstrating that a typical accuracy of 10 meV can be achieved with this setup. For the (100) surface, a quadratic $p(2\times2)$ surface cell is chosen, and the (111) surface is modeled by a rectangular $2\times\sqrt{3}$ $[c(2\times4)]$ cell, which corresponds to a total of 16 Ni atoms in both supercells. For both slabs, a $4\times4\times1$ *k*-point grid is used.

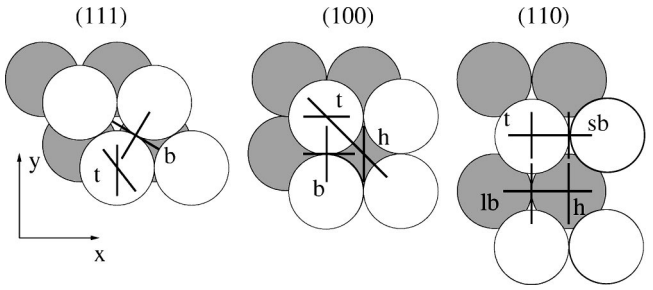

FIG. 1. Representation of the (111), (100), and (110) surfaces indicating the sites and the orientations for which 2D sections of the 6D potential energy surface were calculated (elbow plots). Each plane for which a section was calculated is indicated by a black line. The center of mass of the molecule was always above one of the high-symmetry sites (situated at the crossing of two lines).

The (110) surface is modeled by a five-layer slab and a $p(2\times2)$ supercell. The larger size of the slab and the lower symmetry required a reduction of the *k*-point grid to $3\times2\times1$. Tests indicate that the errors remain smaller than about 40 meV with this setup (in the entrance channel errors remain even smaller than 5 meV). All calculations are performed spin polarized, since in our previous work we found that the adsorption energies per H atom change by about 100 meV if spin polarization is not taken into account.

The present supercells are twice as large as those usually employed in the calculation of hydrogen dissociation on metal surfaces (see, e.g., Refs. 1, 2, and 31). This setup was chosen, because otherwise different supercells must be adopted for different orientations of the incoming molecule. This would make the setup of the calculations generally more tedious, and in some cases it would require one to use incommensurable *k*-point grids for different molecular orientations.

For the present supercells, the interaction between repeated H_2 molecules is fairly small particularly along the entrance channel of the reaction. As will be shown, the entrance channel, where the accuracy is best, turns out to determine the sticking coefficient of H_2 on Ni.

C. 2D sections of the 6D energy surface

For the evaluation of the sticking coefficient, the parametrization of the 6D PES is of crucial importance. Since it is obviously impossible to map out the complete PES exactly, more approximate procedures must be adopted. One such procedure is now discussed, and the final method adopted in this work will be described in Sec. II E.

To describe the position of the molecule the six coordinates x, y, z, d, θ, and ϕ are used. The coordinates x, y, and z describe the position of the center of mass, where z is the distance from the surface plane. The orientation of the x and y axes is shown in Fig. 1. d is the distance between the two H atoms, θ the angle between the surface normal and the axis of the molecule, and ϕ the angle between the x axis and the axis of the molecule projected onto the surface plane. The usual approach—adopted here as well—is based on first-principles calculations of 2D sections of the 6D energy surface. For one such section, the orientation of the molecule

(θ and ϕ) and the coordinates of the center of mass in the surface plane (x,y) are kept fixed. Only the height z and the bond length d vary.

The 2D potentials calculated in this way have an elbow shape so that they are usually called *elbow plots*. For the three Ni surfaces, such 2D sections are evaluated above different high-symmetry sites (i.e., x and y vary) and for different molecular orientations (ϕ and θ vary) as indicated in Fig. 1. For the (111) surface, only the top (t) and bridge (b) sites are used for the parametrization, whereas for the (100) and (110) surfaces the hollow (h) site was also considered. On the (110) surface, one has to distinguish in addition between the long bridge (lb) and the short bridge (sb). At each site, the scans were performed for three different orientations of the molecule; one upright (end on) approach ($\theta=0$) and two flat approaches (side on) with the axis of the molecule parallel to the surface ($\theta=90$).

For a single elbow scan, approximately 200 total energy points were calculated. The height of the molecule varied between 0 Å and 4.2 Å in steps of 0.3 Å , and the distance between the two H atoms was expanded from 0.6 Å to about 3.0 Å in steps of 0.2 Å . The 2D energy surface was interpolated using cubic piece wise continuous polynomials (energies and forces are used) and analytically continued for distances up to 5.0 Å from the surface. This procedure yields a very accurate description of the potential energy surface for one 2D section of the 6D energy surface. The crucial question is obviously how to interpolate between the 2D sections in the remaining four dimensions (x,y,θ,ϕ).

D. Interpolation in the remaining four dimensions

The procedure of the previous section yields a set of three 2D functions for each high-symmetry site, which will be denoted as

$$E_o^{ij}(z,d). \tag{1}$$

Here the indices ij and o label the high-symmetry site and the orientation, respectively. The functions for the upright orientation are given by $E_{\rm up}^{ij}(z,d)$, and the functions for a flat approach are written as $E_{\phi_1}^{ij}(z,d)$ and $E_{\phi_2}^{ij}(z,d)$, where the angles ϕ_1 and ϕ_2 indicate the orientation of the molecule with respect to the x axis (ϕ_1 and ϕ_2 are different for each high-symmetry site). The coordinates of the corresponding high-symmetry sites are given by

$$\vec{r}_{ij}=\frac{i}{N_1}\vec{a}_1+\frac{j}{N_2}\vec{a}_2,$$

$$i=0,\ldots,N_1-1 \quad \text{and} \quad j=0,\ldots,N_2-1,$$

where $\vec{a}_1$ and $\vec{a}_2$ are vectors spanning the *primitive* surface cell. In the present calculations, N_1 and N_2 are 2, and ij can take the values 00, 01, 10, and 11. The position 00 will correspond to the top site. Then the positions 01 and 10 correspond to bridge sites, and on the (100) and (110) surface the index 11 relates to the hollow site. On the (111) surface, the position 11 corresponds to a third bridge site.

The most obvious way to obtain the 6D potential is a simple angular interpolation with respect to θ and ϕ and a Fourier interpolation with respect to the points of impact (x,y). More explictly such a procedure works along the following lines: to obtain the energy of a hydrogen molecule with the coordinates (x,y,z,d,θ,ϕ), one first interpolates the energy with respect to θ and ϕ for *each* high-symmetry site ij:

$$\overline{E}^{ij}=\cos^2\theta\,E_{\rm up}^{ij}(z,d)+\sin^2\theta\left[\cos^2\left(\frac{\pi}{2}\frac{\phi-\phi_1}{\phi_2-\phi_1}\right)\times E_{\phi_1}^{ij}(z,d)+\sin^2\left(\frac{\pi}{2}\frac{\phi-\phi_1}{\phi_2-\phi_1}\right)E_{\phi_2}^{ij}(z,d)\right]. \tag{2}$$

For the positions $(x,y)=x_1\vec{a}_1+x_2\vec{a}_2$ in the surface plane, the energy of a hydrogen atom is then obtained by a Fourier interpolation of the energies $\overline{E}^{ij}$:

$$E_{\rm H_2}=\sum_{k_1=0}^{N_1-1}\sum_{k_2=0}^{N_2-1}a_{k_1k_2}\cos(2\pi k_1x_1)\cos(2\pi k_2x_2),$$

$$a_{k_1k_2}=\frac{1}{N_1N_2}\sum_{n_1=0}^{N_1-1}\sum_{n_2=0}^{N_2-1}\overline{E}^{n_1n_2}\cos\left(2\pi\frac{n_1k_1}{N_1}\right)\times\cos\left(2\pi\frac{n_2k_2}{N_2}\right). \tag{3}$$

It should be noted that the forces can be calculated analytically for this representation of the 6D PES.

Although this procedure is fairly simple it does not lead to a satisfactory representation of the 6D PES. To give one important illustration: at high-symmetry sites, either the flat or the upright approach is energetically most favorable. Inspection of Eq. (2) shows that $\overline{E}^{ij}$ has extremal points at $\theta=0$ and $\theta=\pi/2$ only, in agreement with the previous observation. Equation (3) maintains this property at low-symmetry sites, although in reality a molecule with the center of mass at an off-symmetry site will prefer neither of these two orientations. Hence, the simple interpolation scheme presented in this section cannot account for the correct behavior above low-symmetry sites. In addition, the elbow scans at different sites differ so substantially close to the surface that a simple Fourier interpolation often gives unreliable results in this region. These two arguments clearly show that one has to seek for better interpolation schemes.

1. Parametrization of the three-dimensional PES of atomic H

To improve the parametrization a strategy is adopted in which the potential energy of individual hydrogen atoms is subtracted first. This requires one to evaluate the three-dimensional (3D) PES of a single hydrogen atom by total energy calculations. Since the hydrogen molecule has a nonmagnetic ground state, the non-spin-polarized H atom was chosen as a reference. In addition, tests indicate that the interpolation of the 6D H_2 PES gives more accurate results if the potential of a non-spin-polarized hydrogen atom is subtracted.

For the calculation of the 3D PES of a single H atom, the same slab geometry as before is used. In the following, the position of the hydrogen atom will be denoted by the coordinates (x,y,z). The coordinate z describes again the height of the hydrogen atom above the surface, and x and y relate to

the position in the surface plane. The energy of the hydrogen atom is evaluated for z varying between -0.6 Å and 3.0 Å in steps of 0.1 Å; the x and y coordinates are given by $\vec{r}_{ij}=(x,y)$:

$$\vec{r}_{ij}=\frac{i}{N_1^{\mathrm{H}}}\vec{a}_1+\frac{j}{N_2^{\mathrm{H}}}\vec{a}_2,$$

$$i=0,\ldots,N_1^{\mathrm{H}}-1 \quad \text{and} \quad j=0,\ldots,N_2^{\mathrm{H}}-1.$$

The integers N_1^{H} and N_2^{H} are chosen to be 8 in the present work. Positions which are related to each other by symmetry are calculated only once. This amounts to 15 to 25 (x,y) pairs, and a total of about 500 energy calculations for each surface. The hydrogen potential is extended to a height of 6 Å assuming an exponential decay of the potential for large distances from the surface.

After subtraction of a potential that describes the strong repulsive interaction for very short H-Ni distances, a Fourier interpolation of the hydrogen potential in the (x,y) plane is performed in a similar way as described in Eq. (3). In the z direction the potential is interpolated with cubic functions. The 3D PES of atomic H is from now denoted as $E_{\mathrm{H}}(x,y,z)$.

E. Improved interpolation of the 6D H_2 PES

For H_2, the actual interpolation procedure adopted in this work is based on the observation that the potential

$$G(\vec{r}_1,\vec{r}_2)=E_{\mathrm{H}_2}(\vec{r}_1,\vec{r}_2)-E_{\mathrm{H}}(\vec{r}_1)-E_{\mathrm{H}}(\vec{r}_2) \tag{4}$$

is almost site independent. In this equation, $\vec{r}_1=(x_1,y_1,z_1)$ denotes the position of the first and $\vec{r}_2=(x_2,y_2,z_2)$ the position of the second H atom in the molecule. I will call this potential the effective hydrogen interaction potential, since it describes the interaction between two hydrogen atoms in the vicinity of the surface. The effective potential is first evaluated for each high-symmetry site:

$$G_o^{ij}(z,d)=E_o^{ij}(z,d)-E_{\mathrm{H}}(\vec{r}_1(z,d))-E_{\mathrm{H}}(\vec{r}_2(z,d)), \tag{5}$$

where the potential $E_o^{ij}(z,d)$ is the two-dimensional H_2 potential obtained by the first-principles calculations, and $\vec{r}_1(z,d)$ and $\vec{r}_2(z,d)$ are the positions of the individual hydrogen atoms in the molecule. The 6D effective potential $G(\vec{r}_1,\vec{r}_2)$ is then obtained by interpolation in the remaining four dimensions as described in Eqs. (2) and (3). The final potential of a hydrogen dimer at an arbitrary point is given by

$$E_{\mathrm{H}_2}(\vec{r}_1,\vec{r}_2)=G(\vec{r}_1,\vec{r}_2)+E_{\mathrm{H}}(\vec{r}_1)+E_{\mathrm{H}}(\vec{r}_2). \tag{6}$$

The important point is that an angular and Fourier interpolation of $G_o^{ij}(z,d)$ is much more meaningful than a direct interpolation of $E_o^{ij}(z,d)$, since the former quantity is only weakly site dependent, as will be discussed in more detail in Sec. III B. It is also important to stress that any 2D section used in the course of the interpolation procedure is exactly reproduced by this method (therefore the wording ''interpolation'' is more appropriate than ''parametrization'').

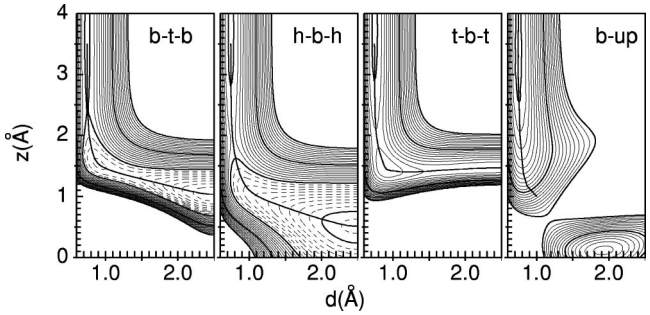

FIG. 2. First-principles results for 2D sections of the PES for dissociative adsorption of H_2 on Ni(100) in various orientations (see text for nomenclature). Contour lines are drawn at intervals of 0.1 eV between −2.0 and 2.0 eV; lines indicating negative (positive) potential energies are dashed (full); thicker lines correspond to integer values. The reaction path is indicated by the line starting at $z=3.5$ Å and $d=0.75$ Å.

F. Evaluation of the sticking coefficient

At this point, accurate 6D representations of the PES's have been obtained. The sticking coefficients are evaluated on these PES's using classical molecular dynamics. Only normal beam incidence is simulated in the present work. Different impact points and different molecular orientations are sampled with a Monte Carlo procedure. The initial vibrational and rotational energies of the molecules are also random and drawn from the simulation of an ideal classical molecular gas at a temperature T, with

$$\frac{5}{2}k_BT=E_{\mathrm{kin}},$$

where E_{kin} is the kinetic energy of the incident molecular beam.[32] The starting height of the molecules is 5 Å, since at this distance the interaction of the molecule with the surface is essentially zero for the present parametrization. The equations of motions are integrated using a Verlet algorithm for a time step of 0.5 fs. The energy stability was typically 0.5 meV, which was found to be sufficient for the present purpose.[33] The simulations are terminated either if the molecule reaches a bond length of 2.0 Å (dissociation) or if the molecule reaches a height larger than 5 Å (reflection). Typically 40 000 trajectories are simulated for each beam energy.

III. RESULTS

A. Elbow scans at selected high-symmetry points

Figure 2 shows the results for 2D sections of the PES for dissociative adsorption of H_2 on Ni(100) as obtained by our first-principles calculations. To distinguish between different orientations, each panel is characterized by three letters x-y-x, where the second letter refers to the center of mass of the molecule and the other two indicate the orientation of the molecule (see also Fig. 1). ''b-t-b'' corresponds to an orientation with both atoms oriented toward bridge sites, where the hydrogen atoms will end up after dissociation. ''b-up'' corresponds to a molecule approaching the surface upright with the center of mass above the bridge site. Also shown is the reaction path $z(s)$ and $d(s)$, along which the gradient of the 2D PES is parallel to the local tangent of the path. In

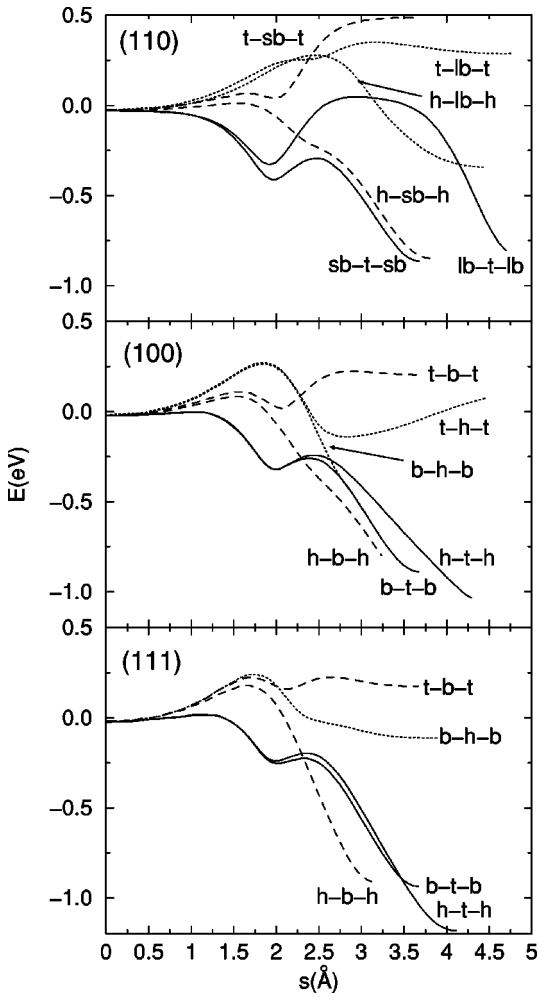

FIG. 3. Potential energy along the reaction path s for H_2 on Ni(110), (100), and (111). The molecules start at a height of 3.5 Å, corresponding to the leftmost point of the diagrams. The energy is shown for an approach over top sites (full lines), bridge sites (dashed lines), and hollow sites (dotted lines). For the (110) surface, the dotted line corresponds to an approach over the long bridge (lb) site (see text for nomenclature).

simple words: if a molecule is dragged slowly from the vacuum toward the surface it follows this pathway exactly. Since the energy along this path allows a simple and direct comparison between different orientations, the potential energies along different reaction pathways are summarized in Fig. 3. In passing, I note that the calculated potential energies along all investigated pathways start at a value 0 ± 5 meV 5 Å above the surface, and they decrease slightly to -20 meV at $z=3.5$ Å. Since the energy along the reaction path is shown from a height of 3.5 Å, all curves have slightly negative values at $s=0$. The shallow energy minimum at a distance of 3 Å might well be a deficiency of the present gradient corrected functionals, but it has no significant influence on the final results (e.g., the sticking coefficient).

I first concentrate on the Ni(100) surface (middle panel of Fig. 3). As can be seen, the most favorable approach is with the center of mass over the top site (full lines, b-t-b and h-t-h). At $s=1.2$ Å, a slight shoulder is visible in Fig. 3, causing an approach of the 0 eV isolines at $z=2.4$ Å in Fig. 2 (b-t-b). The energy then decreases along the reaction path reaching a local minimum at a bond length of 0.9 Å approximately 1.5 Å above the surface. After surmounting a barrier of 60 meV, dissociation into the two bridge sites occurs. For dissociation in the h-t-h orientation, the elbow plot (not shown) and the potential energy along the reaction path are very similar as for b-t-b, but the final energy gain is larger since the atoms end up in the more favorable hollow sites.

Dissociation over the bridge site is accompanied by larger barriers (0.15 eV). This is clearly visible in the elbow plots (h-b-h and t-b-t in Fig. 2) and in Fig. 3 (dashed lines). In this case, the molecule can dissociate only if the atoms are oriented toward the hollow sites, since adsorption of atomic H in the atop position is highly unfavorable (compare Ref. 26). A similar behavior is also found if the center of mass is over the hollow site, but the barrier for dissociation increases even to 0.35 eV (dotted lines, Fig. 3). Finally, no dissociation is observed if the axis of the molecule is parallel to the surface normal (upright approach), since after a slight decrease of the energy at distances of 3.0 Å, the energy essentially increases along the reaction path (Fig. 2, b-up). This increase is steepest for the atop approach and smallest if the molecule is over the hollow sites.

The other two low-index surfaces show in many respects a similar behavior so that the discussion is limited to the energy along the reaction path. For this purpose the results for three important pathways—b-t-b, h-b-h, and b-h-b—are compiled in Fig. 4, now comparing the same pathway for different surfaces in one panel (the results for Pd will be discussed in Sec. IV). For the (111) surface, the approach over the top site is again most favorable, but the barriers are slightly larger than on the (100) surface (see panel b-t-b, Fig. 4). The same is true for an approach over the bridge site (panel h-b-h, Fig. 4), whereas for the hollow sites the barriers have decreased slightly (panel b-h-b, Fig. 4). For the (110) surface, the opposite trend is visible. Now, over the top and the short bridge sites the energy has decreased compared to the (100) surface, whereas over the long bridge and hollow sites a significant increase of the barriers is found. Dissociation over the top site remains the most favorable path (sb-t-sb), but the barrier over the short bridge site is now also very small (h-sb-h, Fig. 3). Figure 3 also shows that the energy along the reaction path is now strongly orientation dependent with significant differences for molecules parallel to the [001] and $[1\bar{1}0]$ direction. The observed trends and, in particular, the height of the barrier along the reaction path will be discussed in more detail in Sec. IV.

B. The effective H-H interaction potential

It is instructive to have a closer look at the effective interaction potential defined in Eq. (5). For this purpose the potential $G^{ij}(z,d)$ for the b-t-b Ni(100) case is shown in Fig. 5. For large distances from the surface (>3 Å), the variation with the bond length d is essentially identical to the binding curve of H_2 (the corresponding isolines are outside the range of values shown in Fig. 5). The energy has a minimum around $d=0.75$ Å at a binding energy of -6.8 eV (with respect to non-spin-polarized H atoms). When the molecule approaches the surface the individual H atoms start to interact with the surface, each gaining about 3.5–4 eV, and at the same time the effective potential between hydrogen atoms

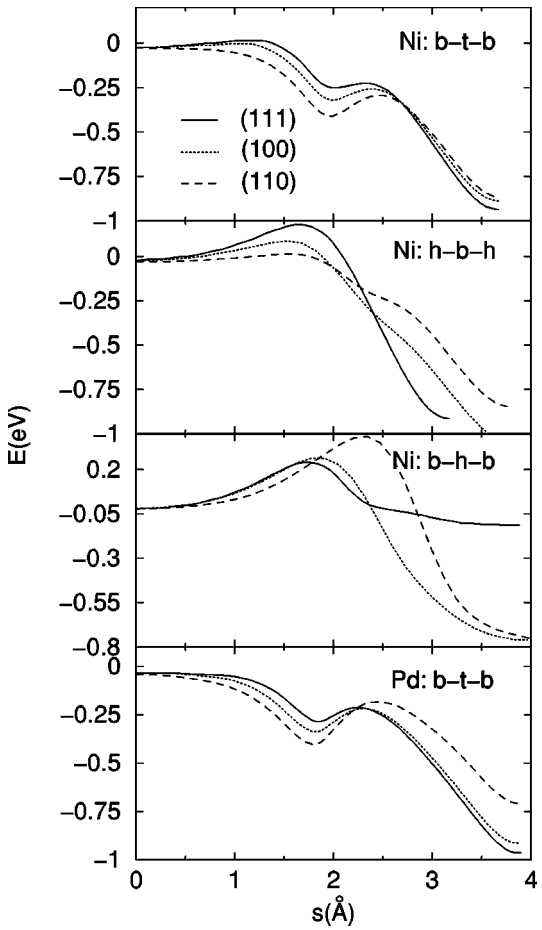

FIG. 4. Potential energy along the reaction path s for selected path ways for H_2 on Ni and Pd (110), (100), and (111). The energy is shown for the b-t-b, h-b-h, and b-h-b orientations. For the (110) surface b corresponds to the short bridge site (see text for nomenclature).

becomes repulsive (remember, positive values in the potential correspond to repulsion). At $d=0.75$ Å and $z=1.0$ Å, a repulsive energy of some 1 eV is found. If, on the other hand, the H-H distance becomes larger than 1.0–1.5 Å the potential becomes effectively zero in the vicinity of the surface, since the two H atoms no longer interact.

The effective interaction potential is very similar for other sites, so that it is more instructive to look at the difference potential $\Delta G = G - G_{\text{b-t-b}}$. For h-b-h and b-h-b, the effective potential is slightly more attractive (negative) at a height of 2.0 Å and a bond length of 0.75 Å. This relates to the fact

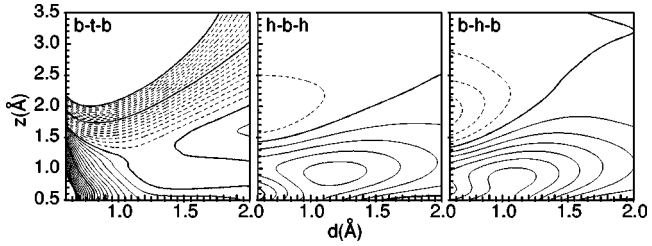

FIG. 5. The effective H-H interaction potential G in the vicinity of the surface for b-t-b, and the difference potentials $\Delta G = G - G_{\text{b-t-b}}$ for h-b-h and b-h-b [Ni (100)]. Contour lines are drawn at the same energies as in Fig 2.

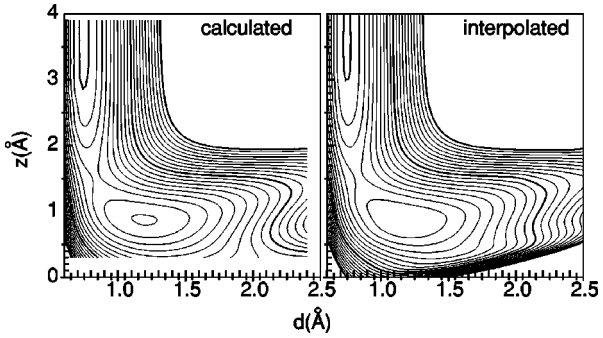

FIG. 6. Comparison of the calculated and interpolated potential energy surfaces for a H_2 molecule over the bridge site of the Ni(100) surface tilted by 60° with respect to the surface normal. Contour lines are drawn at the same energies as in Fig 2. The energy increases along the reaction path, and a shallow local minimum at $z=0.8$ Å, $d=1.2$ Å, and $E\approx 0.1$ eV is found.

that the interaction with the surface starts later for dissociation over the bridge and hollow sites, so that the H-H repulsion over these sites develops more slowly than over the top site. On the other hand, close to the surface, the H-H interaction is now more repulsive (positive). This can be explained by recalling, that adsorbed H atoms carry a negative charge density, which is partially screened by the Ni surface atoms (compare Ref. 26). For dissociation over the top site, a Ni surface atom is located between the two dissociated H atoms, which leads to a reduction of the barriers. For dissociation over the bridge and hollow sites, screening is much less effective, leading to a longer ranged H-H repulsion after dissociation.

C. Interpolation of the potential energy surface

The previous section demonstrates that the effective potential is indeed only weakly site dependent, and that the site dependency can be understood on simple grounds. With this in mind, one can be confident that it is sufficient to parameterize the effective potential at the hollow and top sites only, since these two points represent opposite extremes. For the (110) surface and the (100) surface, the effective potential was also calculated at the bridge site, which should further improve the quality of the parametrization. In the present work, for the (111) surface only the top and bridge sites were used in the interpolation.

To test the accuracy of the interpolation procedure in detail two results are shown. In Fig. 6, the elbow plot for a molecule that is tilted by 60° with respect to the surface normal is presented (h-b-h orientation). The left and right panels show the first-principles results (not used in the course of the parametrization) and the results of the interpolation procedure, respectively. Clearly a very good agreement is found, and inspection of the energy along the reaction path shows a maximum error of 20 meV. Similar tests were performed for other high-symmetry sites, and in all inspected cases the interpolation error with respect to θ remains smaller than 20 meV. With respect to the variable ϕ the accuracy is usually even better, since the ϕ dependence is negligible on the (111) and (100) surfaces. One can conclude that the interpolation procedure gives an accuracy of about 20 meV with respect to the angular interpolation.

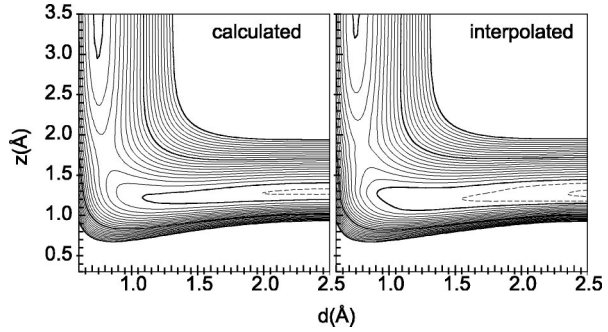

FIG. 7. Comparison of the interpolated and calculated potential energy surfaces for a flat H_2 molecule over the threefold hollow site of the Ni (111) surface (b-h-b). Contour lines are drawn at the same energies as in Fig 2. A barrier of about 0.25 eV is found along the entrance channel.

The inaccuracies are slightly larger for spatial interpolation in the *x* and *y* directions. In Fig. 7, the interpolated b-h-b path on the (111) surface is compared to first-principles calculations (again not included in the parametrization). The error in the interpolated potential is 30 meV up to the barrier and increases to 60 meV after the barrier. The error after the barrier is related to the fact that the electrostatic repulsion between H atoms is underestimated if the center of mass is over the hollow site, since for the (111) surface this approach has not been included in the course of the interpolation. Because the hollow site exhibits relatively large barriers, dissociation over this site is unlikely anyway so that one can probably neglect these inaccuracies.

More generally, the errors seem to be acceptable, in particular if one considers that the current calculations have an absolute accuracy between 10 meV [(111) and (100) surfaces] and 40 meV [(110) surface]. Further tests at low-symmetry sites will be presented elsewhere, and confirm that the accuracy of the angular and spatial interpolation is 20 to 50 meV. Since the errors are in addition generally very small in the entrance channel and become large only at a bond length where dissociation has already occurred, the sticking coefficient should not be affected significantly by these inaccuracies.

D. Sticking coefficients

The final sticking coefficients for the three low index surfaces are summarized in Fig. 8. The calculations were performed classically on the parametrized 6D potential energy surfaces, and 40 000 trajectories were simulated for each beam energy and surface (see Sec. II F for more details). The most important result is that the sticking coefficient shows an activated behavior for the (111) surface and a nonactivated behavior for the (110) surface. This is in accord with the potential energy along the reaction path for the top site [see Fig. 4(b)], where no barrier for dissociation was found on the (110) surface and a notable barrier for the (111) surface. Inspection of the trajectories for the (110) surface shows that at low kinetic energies all molecules are steered toward the top site and dissociate from there into the short bridge sites. In the simulations, the residence time at the top site is often several picoseconds since the molecules have to reorient before dissociation can occur. The mechanism that decreases

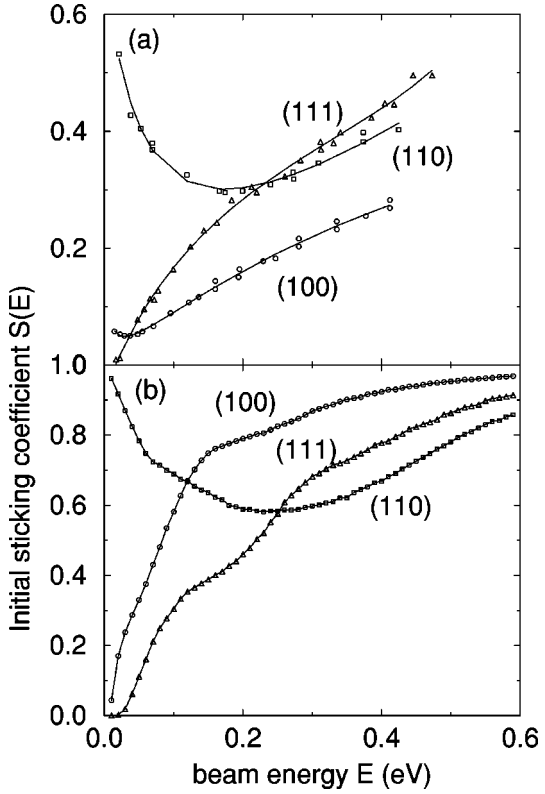

FIG. 8. (a) Experimental and (b) simulated sticking coefficients for H_2 on Ni(111) (triangles), (100) (circles), and (110) (squares). Experimental data are from Ref. 7.

the sticking coefficient with increasing beam energy works exactly along the lines discussed in previous work:[4,5] with increasing energy the molecules do not have sufficient time to reorient or move toward the favorable top site, so that they are reflected by the surface. The increase of the sticking coefficient at around 0.25 eV is related to the fact that new dissociation sites become available at this energy. These are first the short bridge sites, and later the long bridge sites. For the investigated beam energies, dissociation over the hollow site remains very unlikely.

On the other hand, on the (111) surface the initial sticking coefficient is zero, since a finite barrier is found along all pathways. In addition, steering effects are generally small, because the PES is only weakly corrugated. The increase of the sticking coefficient is related to the fact that more sites become available with increasing beam energy. In particular, the barriers over the bridge and hollow sites can be overcome at an energy of around 0.2–0.25 eV, causing a weak shoulder in the curve.

For the (100) surface, essentially no barrier in the entrance channel is observed. The initial sticking coefficient is finite but small and rises steeply with increasing beam energy. On this surface, steering is found to be fairly important at low beam energies (0.1 eV). Most molecules are directed toward the top site and the atoms dissociate from there into hollow and bridge sites. This effect increases the sticking coefficient significantly over that on the less corrugated (111) surface. At around 0.15 eV, the sticking coefficient levels off, since steering becomes less effective, but it starts to increase again at around 0.25–0.3 eV, since then all sites become available for dissociation. The high sticking coeffi-

cient on the (100) surface is therefore related to a combination of steering at low energies and direct activated dissociation at high beam energies.

Coming now to the comparison with experiment, one notes that from a qualitative point of view, the simulations are in satisfactory agreement with the available data. The simulations show the experimentally observed activated behavior for the (111) surface and a nonactivated sticking on the (110) surface. The (100) surface lies—also in agreement with experiment—between these two extremes, although the detailed shape of the curve differs from that found in experiment. In addition, the quantitative agreement between experiment and theory is not satisfactory for any of the three surfaces: for the (111) and (110) surfaces, the simulated sticking coefficient is about twice as large as in the experiment, and the factor seems to become even larger for the (100) surface. The discrepancy between theory and experiment for the (100) surface should not be overinterpreted, since the Ni(100) surface might have been contaminated by CO.[34] Therefore at present the significant overestimation of the sticking coefficient for the other two surfaces seems to require explanation. One point, which has to be kept in mind, is that classical simulations often tend to overestimate the sticking coefficient,[14,15] in particular, if zero point vibrations are not correctly accounted for. It seems likely that some of the discrepancies could be removed by a full QM treatment of the H_2 molecule. I will come back to this point in Sec. V.

IV. DISCUSSION

Certainly, the most apparent result of the present work is the variation of the dissociation barriers with the surface. We first limit our discussion to Ni, and will comment on the Pd surface only in the last paragraph of this section.

Over the top site and for a distance of 2.2 Å from the surface, the H_2 molecule is about 70 meV more stable on the (110) surface than on the (111) surface. The energy difference increases to 150 meV for smaller distances (compare Fig. 4), but changes sign at very small distances. One must stress here that surface magnetism does *not* change these results significantly, which was established by repeating the b-t-b calculations for an artificial nonmagnetic Ni surface: for the first part of the reaction pathways, the energies remain essentially unchanged, and, in particular, the barrier on the (111) surface is not reduced. The decrease of the dissociation barriers from the close packed to the more open surface is also observed for other *d* metals, for instance, Cu (111) and Cu (110).[35] But, interestingly in our case, the decrease of the dissociation barrier over the top site is accompanied by a significant increase of the barriers over the hollow and lb sites. In other words, the (111) surface exhibits only a fairly small corrugation, whereas the corrugation is large on the (110) surface. To explain this behavior, I will partly rely on a model developed in Ref. 35, but as will be discussed below the effect of the *s* electrons seems to be more important than assumed so far in the literature.[16,17] This section will also compare the current results with those for H_2 on Pd.[1,2,31,36–38] To make this comparison less dependent on technical parameters, the PES's of H_2 on all three Pd surfaces were recalculated with essentially the same setup as for Ni.

To discuss the dissociation of H_2 on a transition metal surface, one has to keep in mind that the electrostatic potential and the surface *s* and *d* electrons play an important role (see Refs. 16, 17, and 35). Let me first concentrate on the surface *s* electrons and the electrostatic potential. When the hydrogen molecule is brought to the surface, the hydrogen electrons gain energy because they experience the surface potential (the H_2 σ level moves to lower energies). This is counterbalanced by the electrostatic repulsion exerted on the H core and the repulsion caused by the overlap of H 1*s* electrons and Ni surface *s* electrons (Pauli repulsion). The net interaction is usually repulsive, since the electrostatic effects balance each other and only the Pauli repulsion survives.

The second contribution stems from the interaction of the Ni *d* electrons with the H_2 molecule. In the usual picture, charge is donated from the H_2 σ orbital to the surface *d* states, accompanied by a back-donation from the surface *d* states to the H_2 σ^* orbital.[16,17] The net effect is a weakening of the H-H bond and a strengthening of the H-substrate bond. Over the top site the Ni $d_{3z^2-r^2}$, d_{xz}, and d_{yz} orbitals interact with the H_2 molecule. The almost fully occupied $d_{3z^2-r^2}$ orbital hybridizes with the occupied H_2 σ orbital, moves to higher energies, and loses a very small amount of charge. For Ni, the effect on the energy is small and probably repulsive (Pauli repulsion), since two initially occupied states interact and remain both almost occupied. The major bonding contribution over the top site derives from the d_{xz} and d_{yz} orbitals. These orbitals extend into the vacuum and are antisymmetric with respect to the H_2 molecule. They experience only the electrostatic potential of the H cores but no Pauli repulsion, since the occupied H_2 σ state is orthogonal to them. Although at large distances from the surface the interaction has mainly an electrostatic origin, the covalent contribution cannot be neglected at smaller distances, when bond breaking occurs.[39,31] As a result of the interaction, the centers of the almost filled d_{xz} and d_{yz} states shift to lower energies and the unoccupied H_2 σ^* orbital moves to higher energies, yielding a net energy gain. Such an antisymmetric contribution of *d* orbitals is predominantly available above the top site. Over the bridge or hollow sites, *d* states that are antisymmetric with respect to the H_2 molecule exist only in small parts of the Brillouin zone. This explains why the approach over top is most favorable. Together with Smoluchowski[40] smoothing we can now also understand why dissociation over the troughs is particularly unfavorable on the (110) surface. Since Smoluchowski smoothing leads to an accumulation of *s* electrons in the troughs, the H_2 dimer experiences a strong Pauli repulsion when it approaches the surface over the hl or lb sites. Together with the absence of antisymmetric *d* orbitals, a strong repulsion between the H_2 dimer and the surface is found.

The picture is corroborated by the local density of states (DOS) shown in Fig. 9. The H_2 σ orbital is located about -7 eV below the Fermi level (full line). For Ni, the *s* and *p* DOS on the surface atom (dotted line) overlaps energetically with the H_2 σ orbital. The surface *d* electrons are found at an energy of -5 to 1 eV (dashed line). As indicated in Fig. 10, the position of the unperturbed σ state with respect to the Fermi level is given approximately by $\epsilon_\sigma - \phi$, where ϕ is the work function. Since the work function is larger for the close

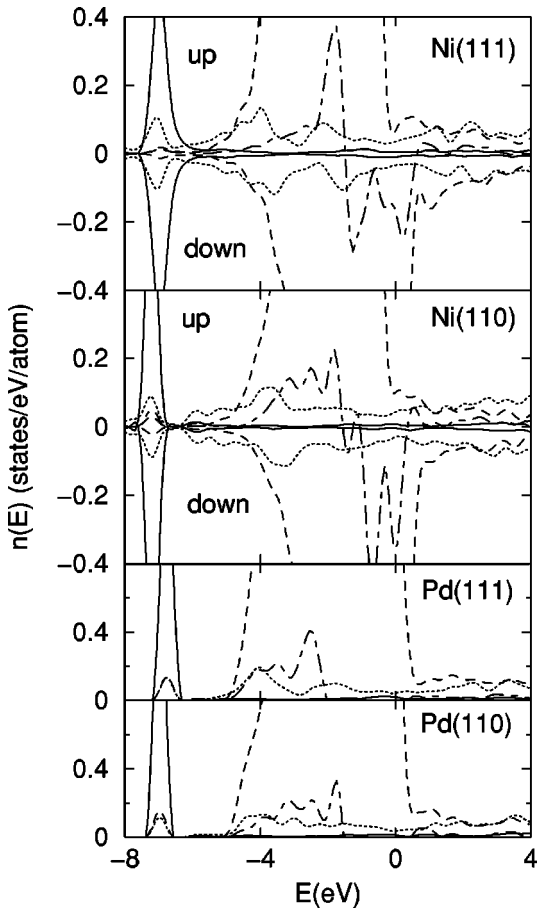

FIG. 9. Local density of states (l-DOS) at the H_2 molecule (full line) and at the transition metal (TM) surface atom for the (111) and (110) surfaces (H_2-surface distance 2.2 Å, b-t-b orientation). The TM *s* and *p* DOS's are shown as dotted and the TM *d* states as dashed lines. The dash-dotted line indicates the change in the DOS of the surface atom compared to the clean surface (summed over up and down).

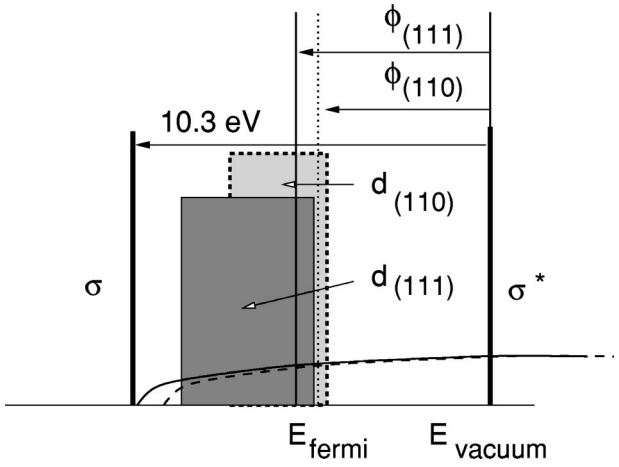

FIG. 10. Schematic DOS for H_2 on Ni. The *d* states are shown as gray rectangles [dark gray, (111) surface, light gray, (110) surface], the position of the Fermi level with respect to the vacuum level is indicated by lines, and the surface *s* states are indicated by a parabola [full lines, (111) surface, dashed lines, (110) surface]. The positions of the σ and σ^* state are shown as thick black lines. The σ orbital is located 10.3 eV below the vacuum level, and the local density approximation σ^* orbital is located approximately at the vacuum level. The position of the σ orbital with respect to the Ni *d* band depends on the work function. Qualitatively similar results are obtained for Pd, but for Pd the σ state does not overlap with the surface *s* states.

packed surface than for the open surface, the σ state is located at lower energies on the (110) than on the (111) surface ($\phi_{(111)}=5.07$ eV; $\phi_{(110)}=4.55$ eV; compare Ref. 26). This has several effects, all reducing the barriers on the (110) surface compared to the (111) surface. First, the interaction between the H_2 σ orbital and the surface *s* electrons is larger on the (111) surface, increasing the Pauli repulsion. As a result the σ state is much broader on the (111) surface than on the (110) surface (cf. Fig. 9). In a similar way, the Pauli repulsion between the σ orbital and the $d_{3z^2-r^2}$ state is reduced on the (110) surface. Finally, the bonding between the d_{zx} and d_{zy} states and the H_2 σ^* orbital is enhanced on the (110) surface, since the *d* band is narrower, and closer to the H_2 σ^* level.

The picture presented here should be relevant for hydrogen dissociation on most transition metals, and it is interesting to compare Ni with Pd. Since Pd has a 40% larger volume than Ni, the *s* bandwidth is significantly reduced in Pd (compare Fig. 9). The reduced *s* density should reduce the Pauli repulsion between surface *s* electrons and the H_2 σ orbital. Figure 9 indeed shows that the *s* and *p* DOS (dotted line) is significantly reduced at the position of the σ orbital (-7 eV, below the Fermi level). Since the *d* electrons—on the other hand—extend further into the vacuum, the interaction between the *d* electrons and the H_2 molecule is enhanced. Both effects combine and lead at large distances to a stronger bonding of H_2 to the substrate. The last panel in Fig. 4 demonstrates that the barrier has vanished on the Pd(111) surface, which is in agreement with the experimental observation that hydrogen dissociation is nonactivated on all three low-index Pd surfaces.[7,41,42] Closer inspection shows that the energy along the reaction pathways changes by the same amount on *all three* surfaces: at a distance of 2.2 Å, the H_2 molecule is about 100 meV more stable on Pd than on Ni. This, of course, causes the barrier to disappear on the (111) surface, but the change is not caused by any feature peculiar to the (111) surface. I conclude that the reduction of the *s* bandwidth and *s* density, which is caused by the increased atomic volume of Pd, is responsible for the vanishing of the H_2 dissociation barriers on Pd.

V. CONCLUSION

The important methodological development of the present work is the introduction of an interpolation scheme for the 6D PES of H_2. Like many previous schemes it relies on the evaluation of 2D sections of the full PES. But to interpolate between these sections, an intermediate effective H-H interaction potential in the vicinity of the surface is introduced. This potential is obtained by subtracting the potential of two individual H atoms from the calculated 2D H_2 PES. The effective potential is only weakly site and orientation dependent and can be Fourier interpolated accurately between high-symmetry sites. The interpolation predicts the correct molecular orientation above low-symmetry sites, which is a significant advantage over previous simpler schemes,[5,31] but

it does not suffer from the functional restrictions other parametrizations have (e.g., the LEPS parametrization). In addition, the first-principles results at high-symmetry sites are exactly reproduced.

With this scheme, a detailed investigation of the PES and the sticking of H_2 on the three low-index Ni surfaces was performed. In a first step, 2D sections of the 6D PES were calculated by first-principles calculations. It is found that dissociation over the top site is most favorable on all three surfaces, but the energies along the reaction pathways differ by up to 150 meV between the three surfaces. Generally, dissociation over the top site of the rougher surface is easier than over the top site of the close packed surfaces, so that no barrier for dissociation is found on the (110) surface and a small barrier of about 15 meV is obtained on the (111) surface. The origin of this variation can be traced back to the position of the H_2 σ and H_2 σ^* orbital with respect to the metal electrons: on the open surfaces, the work function is smaller, shifting the H_2 states to lower energies. As a result the Pauli repulsion between the H_2 σ orbital and the Ni *s* and *d* states is reduced, and the bonding interaction between the H_2 σ^* and *d* states increases. A comparison between Ni and Pd indicates that the Pauli repulsion between the metal *s* electrons and the H_2 σ orbital is much stronger on Ni than on Pd. This observation explains why dissociation of H_2 is activated on Ni (111) and nonactivated on Pd(111).

The decrease of the barrier over the top site on the rough (110) surface is accompanied by a significant increase of the dissociation barriers over the troughs. In other words, the structurally roughest surface is also electronically strongly corrugated. The trends in the barriers and in the corrugation strongly affect the dissociation dynamics on the three surfaces. On the flat uncorrugated (111) surface steering is not very important. Initially the sticking coefficient is effectively zero, and sticking increases with increasing beam energy. The observed increase is mainly related to the opening of dissociation channels with increasing translational energy. This agrees well with previous experimental interpretations.[7] On the (100) surface, the corrugation is larger than on the (111) surface, and in addition no barrier is found for dissociation over the top site. Steering now plays an important role, in particular at low kinetic energies. At a beam energy of 0.1 eV, most molecules are directed towards the top site where they dissociate quickly. At higher kinetic energies, the surface behaves like the flat uncorrugated (111) surface, since with increasing beam energy more sites become available for dissociation. Finally, on the rough (110) surface, dissociation occurs exclusively above the close packed Ni rows. At low kinetic energies it is again mainly the reaction path over the top site that is utilized, but with increasing beam energy the short bridge site also becomes available. Since dissociation over the troughs is very unfavorable, steering is now a dominant mechanism even at intermediate and high beam energies.

The simulated sticking curves are in qualitative agreement with previous experiments, but unfortunately the quantitative agreement is not so good. For a wide range of energies, the sticking coefficient is overestimated by about a factor of 2. At present, it is unclear whether this is related to uncertainties of the experimental data or to inaccuracies of the present approach. Although it is well known that the absolute magnitude of the sticking coefficient is difficult to determine experimentally, I want to address briefly possible deficiencies and advantages of the present approach.

Since the interpolation scheme is very accurate it seems unlikely that errors are caused by an inappropriate representation of the PES. On the contrary—all previous high-dimensional QM studies (and most classical simulations) utilized parametrizations that did not account for the fact that the H_2 molecules will tend to tilt over low-symmetry sites.[4,5,31] An interesting application of the interpolation scheme presented here is to investigate how large these effects are, and such calculations are currently in progress.

The most likely reason for the discrepancy between theory and experiment is therefore the classical treatment of the H_2 molecule. In previous work, it has been shown that such a treatment often increases the sticking coefficient compared to a full QM treatment of the H_2 molecule.[15] Unfortunately, such QM simulations would be extremely time consuming, since the current parametrization allows for a scattering by odd *m* quantum numbers, which increases the computational effort of the QM calculations by a factor of 8 compared to previous calculations.[43] The lower symmetry of the (110) surface further increases the computational demands. Despite these difficulties, I hope to come back to this point in future work.

Recently, a similar interpolation scheme was suggested by Busnengo, Salin, and Dong and applied to the dissociation of H_2/Pd(111).[44]

ACKNOWLEDGMENTS

I thank A. Eichler and J. Hafner for helpful discussions and comments. The initial stage of this work was supported by the Austrian Science Funds within the Joint Research Project on Gas-Surface Interaction, Grant No. S8106-PHY.

[1] S. Wilke and M. Scheffler, Surf. Sci. **329**, L605 (1995).
[2] S. Wilke and M. Scheffler, Phys. Rev. B **53**, 4926 (1996).
[3] J.A. White, D.M Bird, and M.C. Payne, Phys. Rev. B **53**, 1667 (1996).
[4] M. Kay, G.R. Darling, S. Holloway, J.A. White, and D.M. Bird, Chem. Phys. Lett. **245**, 311 (1995).
[5] A. Groß and M. Scheffler, Phys. Rev. Lett. **77**, 405 (1996).
[6] C.T. Rettner and D.J. Auerbach, Chem. Phys. Lett. **253**, 236 (1996).
[7] K.D. Rendulic, G. Anger, and A. Winkler, Surf. Sci. **208**, 404 (1989).
[8] C.Y. Lee and A.E. DePristo, J. Chem. Phys. **85**, 4161 (1986); J. Vac. Sci. Technol. A **5**, 485 (1987); J. Chem. Phys. **87**, 1401 (1987).
[9] A. Bourcet and G.F. Tantardini, J. Electron Spectrosc. Relat. Phenom. **69**, 55 (1994).
[10] H. Sellers, J. Chem. Phys. **101**, 5201 (1994).
[11] R.C. Mowrey, J. Chem. Phys. **99**, 7049 (1993).

[12] P. Sallfrank and W.H. Miller, J. Chem. Phys. **98**, 9040 (1993).
[13] M.S. Munn and D.C. Clary, J. Chem. Phys. **105**, 5258 (1996).
[14] M. Kay, G.R. Darling, and S. Holloway, J. Chem. Phys. **108**, 4614 (1998).
[15] A. Gross and M. Scheffler, Phys. Rev. B **57**, 2493 (1998).
[16] B. Hammer and J.K. Norskov, Nature (London) **376**, 238 (1995).
[17] B. Hammer and J.K. Norskov, Adv. Catal. (to be published).
[18] W. Kohn and L. Sham, Phys. Lett. **140**, A1133 (1965).
[19] R.O. Jones and O. Gunnarsson, Rev. Mod. Phys. **61**, 689 (1989).
[20] R. Car and M. Parrinello, Phys. Rev. Lett. **55**, 2471 (1985).
[21] M.C. Payne, M.P. Teter, D.C. Allan, T.A. Arias, and J.D. Joannopoulos, Rev. Mod. Phys. **64**, 1045 (1992).
[22] G. Kresse and J. Hafner, Phys. Rev. B **48**, 13 115 (1993).
[23] G. Kresse and J. Furthmüller, Comput. Mater. Sci. **6**, 15 (1996); Phys. Rev. B **54**, 11 169 (1996).
[24] P.E. Blöchl, Phys. Rev. B **50**, 17 953 (1994).
[25] G. Kresse and D. Joubert, Phys. Rev. B **59**, 1758 (1999).
[26] G. Kresse and J. Hafner, Surf. Sci. **459**, 287 (2000).
[27] Y. Wang and J.P. Perdew, Phys. Rev. B **44**, 13 298 (1991).
[28] J.P. Perdew, J.A. Chevary, S.H. Vosko, K.A. Jackson, M.R. Pederson, D.J. Singh, and C. Fiolhais, Phys. Rev. B **46**, 6671 (1992).
[29] H.J. Monkhorst and J.D. Pack, Phys. Rev. B **13**, 5188 (1972).
[30] M. Methfessel and A.T. Paxton, Phys. Rev. B **40**, 3616 (1989).
[31] A. Eichler, G. Kresse, and J. Hafner, Surf. Sci. **397**, 116 (1998).
[32] G. Anger, A. Winkler, and K.D. Rendulic, Surf. Sci. **220**, 1 (1989).
[33] Tests with a smaller time step and better energy conservation yield identical sticking coefficients.
[34] K.D. Rendulic (private communication).
[35] P. Kratzer, B. Hammer, and J.K. Norskov, Surf. Sci. **359**, 45 (1996).
[36] A. Eichler, J. Hafner, A. Groß, and M. Scheffler, Phys. Rev. B **59**, 13 297 (1999); Chem. Phys. Lett. **311**, 1 (1999).
[37] W. Dong, G. Kresse, and J. Hafner, J. Mol. Catal. A: Chem. **119**, 69 (1997).
[38] V. Ledentu, W. Dong, and P. Sautet, Surf. Sci. **412**, 518 (1998).
[39] A. Eichler, G. Kresse, and J. Hafner, Phys. Rev. Lett. **77**, 1119 (1996).
[40] R. Smoluchowski, Phys. Rev. **60**, 661 (1941).
[41] Ch. Resch, H.F. Berger, K.D. Rendulic, and E. Bertel, Surf. Sci. **316**, L1105 (1994).
[42] M. Beutl, M. Riedler, and K.D. Rendulic, Chem. Phys. Lett. **247**, 249 (1995).
[43] A. Gross (private communication).
[44] H. F. Busengo, A. Salin, and W. Dong, J. Chem. Phys. **112**, 7641 (2000).